Geophys. J. Int. (2001) **146,** 747–759

Evolution of the stress field in the northern Aegean Sea (Greece)

Eleftheria E. Papadimitriou[1] and Lynn R. Sykes[2,3]

[1] *Department of Geophysics, University of Thessaloniki,* GR54006 *Thessaloniki, Greece. E-mail: ritsa@geo.auth.gr*
[2] *Lamont-Doherty Earth Observatory, Columbia University, Palisades, New York,* NY 10964, *USA. E-mail: sykes@ldeo.columbia.edu*
[3] *Department of Earth and Environmental Sciences, Columbia University, New York, USA*

Accepted 2001 April 16. Received 2001 March 8; in original form 2000 March 20

SUMMARY

The evolution of the stress field in the area of the northern Aegean Sea during the 20th century has been studied. The area is dominated by dextral strike-slip faulting and is characterized by frequent strong earthquakes. Coulomb stress changes (ΔCFF) were calculated assuming that earthquakes can be modelled as static dislocations in an elastic half-space, and taking into account both the coseismic slip in large ($M \geq 7.0$) earthquakes and the slow tectonic stress build-up along the major fault segments. The stress change calculations were performed for strike-slip faults of strike, dip, and rake appropriate to the large events. We evaluate whether these stress changes brought a given large earthquake closer to, or farther from, failure. It was found that each of the large events occurred in regions of increased calculated Coulomb stress. Moreover, the majority of smaller events for which reliable fault-plane solutions are available were also located in areas of positive ΔCFF. By extending the calculations to 2020, and assuming that no additional large ($M \geq 7.0$) earthquake occurs between 1999 and 2020, possible sites of future large earthquakes are identified.

Key words: North Aegean Sea, stress evolution, strike-slip faulting.

1 INTRODUCTION

The area of the northern Aegean Sea (Greece) has experienced many destructive earthquakes as indicated by both instrumental data and historical information. It constitutes the northern boundary of the south Aegean plate (Papazachos *et al.* 1998) and is a continuation of the western part of the North Anatolian fault. Strike-slip dextral faulting dominates this region as the North Anatolian fault prolongates into the north Aegean area, where it bifurcates into two main branches of NE–SW trend. Parallel secondary faults are also recognized from seismicity and fault-plane solutions of recent strong earthquakes.

This area has frequently experienced large ($M \geq 7.0$) earthquakes, some of them occurring very close together in time. It is, then, of interest to examine whether the stress changes associated with the occurrence of each of them can advance the time of occurrence of, i.e. trigger, subsequent ones. Earthquakes in a sequence generally are not independent (Scholz 1990). Each one is affected by both tectonic loading and stress changes caused by prior events, especially by either great earthquakes or other shocks that occur nearby. From this point of view, the state of stress and its variation with time are studied.

Seismicity rate decreases have been successfully identified in situations where faults were relaxed, the result of a negative change in Coulomb failure stress, $\Delta CFS < 0$. For cases where a fault is relaxed, or put into a stress shadow (Harris & Simpson 1993, 1996; Deng & Sykes 1997a,b), one can perform simple determinations of the approximate time that it should take for long-term tectonic loading to recover the static stress change. The time change, now a delay, is simply expressed as $\Delta CFS/\dot{\tau}$, where $\dot{\tau}$, the long-term stressing rate, is the time required to bring the fault back to its state of stress before relaxation. Simpson *et al.* 1988) estimated that the 1983 Coalinga earthquake delayed the next moderate Parkfield earthquake on the San Andreas Fault in central California by at least 1 year. This technique of using Coulomb stress changes to estimate time delays has also been applied to larger earthquakes. Simpson & Reasenberg (1994) and Jaumé & Sykes (1996) calculated the effects of the great 1906 San Francisco earthquake on nearby active faults. The 1906 earthquake, which ruptured the San Andreas Fault in central and northern California, relaxed many of the San Francisco Bay area's faults and is proposed to have delayed subsequent large earthquakes for decades (Harris & Simpson 1998). Simpson & Reasenberg (1994) determined that, after 1906, moderate to large earthquakes on nearby faults largely ceased, and then began again later at a time consistent with models of long-term tectonic reloading. They also made estimates of the effects of the large 1989 Loma Prieta earthquake on nearby San Francisco Bay area faults. Lienkaemper *et al.* (1997) validated these estimates by showing that a recent resumption of creep on the Hayward fault is consistent with tectonic erosion of the 1989 stress shadow.

An attempt is made here to examine the evolution of the stress field in the area of the northern Aegean Sea during the 20th century. For this time interval, epicentral determinations and fault-plane solutions are more reliable for the larger events. Previous work for the same area has been done by Nalbant *et al.* (1998) for coseismic stresses associated with the largest earthquakes; changes in stress generated by tectonic loading, however, were not included in their study. In the present paper, both coseismic stress changes associated with the occurrence of large ($M \geq 7.0$) earthquakes and slow tectonic stress accumulation along major faults in the area are taken into account, following the procedure of Deng & Sykes (1997a). In this way it is possible to examine if the history of cumulative changes in stress can explain the spatial and temporal occurrence patterns of large northern Aegean Sea earthquakes and perhaps bring about new insights into the estimation of future seismic hazards.

2 METHOD

We used the method of Deng & Sykes (1997a), which considers stress to be a tensor quantity that varies in time and space and is transmitted elastically within a homogeneous half-space earth. According to this method, cumulative changes in stress are assumed to arise from two sources: tectonic loading generated by plate motions and coseismic displacements on faults associated with large earthquakes. Interseismic stress accumulation between large events is modelled by introducing 'virtual negative displacements' along major faults in the entire study region using the best available information on long-term slip rates. Hence, tectonically induced stress builds up in the vicinity of faults during the time intervals between earthquakes. All computed interseismic stress accumulation is associated with the deformation caused by the time-dependent virtual displacement on major faults extending from the free surface to the seismogenic depth, namely the depth at which earthquakes and brittle behaviour cease ($\sim$15 km depth). Stress build up is released wholly or in part during the next large to great earthquake, with real displacements on given fault segments that are considered positive in the model.

We make the assumption that stress changes can be modelled as those caused by elastic strain accumulation and release during the earthquake cycle. Our basic assumption is that the static stress change at the time of a large earthquake is completely recovered during the period of strain accumulation; that is, the net change in stress over the earthquake cycle is zero. This assumption is equivalent to the time-predictable model of earthquake occurrence (Shimazaki & Nakata 1980). The natural 'base level' from which we start our stress evolution model is the instant before failure in a large earthquake, when stress has reached the failure level. The evolution of the stress field is then the coseismic stress change resulting from the large earthquake followed by the evolution of the stress field as tectonic strain is accumulated within the study area.

Changes in stress associated with large to great earthquakes are calculated by putting coseismic displacements on ruptured fault segments in the elastic half-space and adding the changes in the components of the stress tensor together as they evolve in time. Stress changes associated with both the virtual dislocations and actual earthquake displacements are calculated using a dislocation model of a planar fault surface, Σ, embedded in a homogeneous semi-infinite elastic medium, namely a half-space with zero traction on the Earth's surface. Steketee (1958) showed that the displacement field u_k (kth component of u) in a semi-infinite elastic medium for an arbitrary uniform dislocation, U, across a surface, Σ, can be determined from

$$u_k = \frac{U_i}{8\pi\mu} \iint_{\Sigma} w_{ij}^k v_j \, d\Sigma \,, \tag{1}$$

where μ is the shear modulus, v_j are the direction cosines of the normal to the dislocation surface, U_i is the ith component of U, and w_{ij}^k are six sets of Green's functions.

The modelled displacements and strain fields associated with the finite rectangular sources are obtained by integrating eq. (1) (Okada 1992; G. Converse, US Geological Survey, unpublished report 1973). The elastic stress s_{ij} is calculated from the strain e_{ij} using Hooke's law for an isotropic medium:

$$s_{ij} = \frac{2\mu v}{1-2v} \delta_{ij} e_{kk} + 2\mu e_{ij} \,, \tag{2}$$

where v is Poisson's ratio, and δ_{ij} is the Kronecker delta.

Earthquakes occur when the stress exceeds the strength of the fault. The closeness to failure was quantified using the change in Coulomb failure function (ΔCFF) (modified from Scholz 1990; Harris 1998 and references therein). It depends on changes in both shear stress $\Delta\tau$ and normal stress $\Delta\sigma$:

$$\Delta\mathrm{CFF} = \Delta\tau + \mu\Delta\sigma \,. \tag{3}$$

Here μ is the apparent coefficient of friction. Both $\Delta\tau$ and $\Delta\sigma$ are calculated from the stress tensor described by eq. (2) for a fault plane at the observing (field) point. The change in shear stress $\Delta\tau$ is positive for increasing shear stress in the direction of slip on the observing fault; $\Delta\sigma$ is positive for increasing tensional normal stress. When compressional normal stress on a fault plane decreases, the static friction across the fault plane also decreases. Positive $\Delta\tau$ and $\Delta\sigma$ move a fault towards failure; negative $\Delta\tau$ and $\Delta\sigma$ move it away from failure. A positive value of ΔCFF for a particular fault denotes movement of that fault towards failure (that is, the likelihood that it will rupture in an earthquake is increased).

The advantage of using changes in stress is that often absolute values of stress are not known but values of stress change can be calculated fairly readily from information about the geometry and slip direction of an earthquake rupture. Furthermore, the exact details of geometry and slip become less important the farther one goes from the rupture (Aki & Richards 1980).

3 PLATE TECTONIC SETTING, FAULTS AND SLIP-RATE CONSTRAINTS

Various researchers have presented much information on the basic problems regarding active tectonics and deformation in the broader Aegean area (Fig. 1). Papazachos & Comninakis (1970, 1971) were the first to suggest that the subduction of the African tectonic plate under the Aegean was related to the northward motion of the African plate with respect to the Aegean and the identification of intermediate-depth earthquakes beneath the southern Aegean. McKenzie (1970, 1972, 1978) showed that the northward motion of the Arabian plate pushes the smaller Anatolian plate westwards along the North Anatolian fault. This motion is transferred into the Aegean but in a south-westerly direction. These motions imply that the northern Aegean is dominated by dextral strike-slip faulting of northeasterly strike.

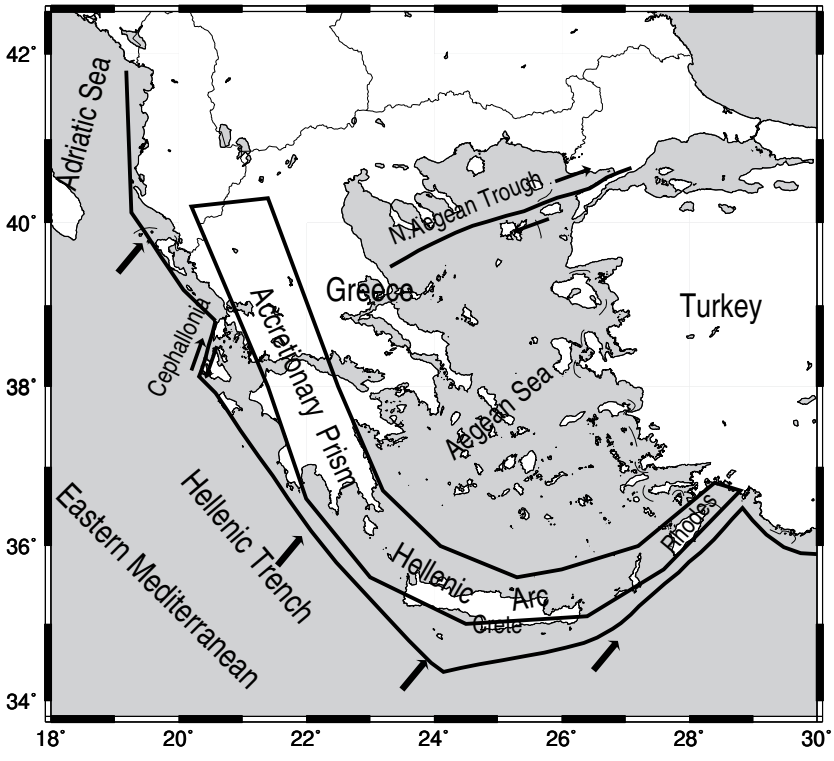

Figure 1. Main seismotectonic properties of the Aegean and surrounding regions.

This style of faulting is consistent with several fault-plane solutions of recent strong earthquakes as well as neotectonic observations.

It has been suggested that the Aegean Sea and much of Anatolia consist of two separate small plates (McKenzie 1972; Jackson 1994). The southern boundary of the south Aegean plate is defined by the low-angle thrust faults of shallow earthquakes that are located along the Hellenic Trench. The mean direction of seismic slip along these faults is in agreement with Global Positioning System (GPS) data that suggest a southwestward motion of the Aegean plate with respect to the Eurasian Plate (e.g. Reilinger *et al.* 1997). The Anatolian plate is moving westwards relative to the Eurasian plate along the North Anatolian Fault, with an average velocity of about $\sim$24 mm yr^{-1} which is accommodated by an additional N–S deformation of $\sim$11 mm yr^{-1} in the Aegean, resulting in a total SW motion of $\sim$41 mm yr^{-1} of the southern Aegean relative to Eurasia. A large part of this deformation occurs seismically, as the Aegean shows a total seismic slip of the order of 20 mm yr^{-1} relative to Eurasia (Papazachos & Kiratzi 1996). A different model has been suggested for the area (LePichon *et al.* 1995; Oral *et al.* 1995; Reilinger *et al.* 1997) derived from mainly GPS observations for Turkey combined with Satellite Laser Ranging (SLR) data for Greece. This model suggests a single Anatolia–Aegean microplate, which performs an almost rigid-body rotation around a pole located in the northern Sinai Peninsula. Papazachos (1999), using two types of data, GPS and seismological, showed that the pattern of deformation in the Aegean area cannot be described by a rigid-body rotation model that best fits the Anatolian–Eurasian relative motion (Fig. 2), confirming the suggestion of Jackson (1994) who used seismological and SLR data. McClusky *et al.* (2000), using more recent GPS data, also conclude that two separate plates—the Anatolian and south Aegean—exist in the area. The rotation of the Anatolian plate is transferred in the Aegean area as a simple translation, indicated by the subparallel deformational field in this area. This translation occurs along the central and southern parts of the coasts of Turkey and the neighbouring Greek islands. The Aegean moves almost uniformly in a SSW direction ($\sim$200°–220°) with an average velocity of $\sim$30 mm yr^{-1}; the velocity increases from 25 mm yr^{-1} in the central and southern part of the western coast of Turkey to 30–35 mm yr^{-1} near the southwestern part of the Hellenic arc (Papazachos 1999). This significant increase is due to the strong N–S extension in the Aegean and western Turkey.

By considering the south Aegean as a separate microplate extending east to 28°E, the major parallel strike-slip faults in the northern Aegean Sea can be defined. Since the examined area is mainly submarine, not much information concerning the surface expression of active faults exists. Results on structural analysis are available only for the island of Agios Efstratios, which was affected by the destructive earthquake of 1968 (Pavlides & Tranos 1991). Deformation at the surface was detected along a NE–SW right-lateral strike-slip fault, over a distance of 3 km. The main structures of Agios Efstratios Island have been mapped using field data and aerial photographs. The fault of the strong earthquake of 1968 trends NE–SW with a strike of 45°, dips to the NW at 81°, and is consistent with focal mechanism solutions. The latter piece of information is evidence that fault-plane solutions found for the strong earthquakes of the area are in agreement with the available geological field observations.

Since field information is sparse, indirect methods are used to define the faults of interest. The North Anatolian fault bifurcates east of the Marmara Sea. Two main branches extend into the northern Aegean region. In addition, several parallel subfaults

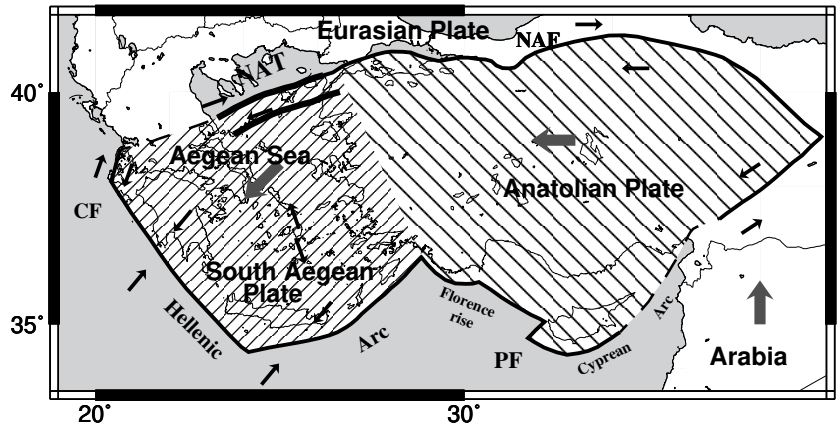

Figure 2. Main geotectonic features of the Aegean–Anatolia area (CF: Cephalonia Fault; NAT: Northern Aegean Trough; NAF: North Anatolia Fault; PF: Paphos Fault). Thick and thin arrows indicate plate motions relative to Eurasia and local motions, respectively (after Papazachos 1999 and McClusky *et al.* 2000).

are recognized from the distribution of seismicity and the occurrence of precisely located strong earthquakes (Papazachos *et al.* 2000). Information about rupture lengths comes from studies of aftershock sequences, since it is accepted that the foci of aftershocks are distributed along the fault surface that ruptured (Beroza 1991). We use recent seismic activity for which precise epicentral determinations are available to define the major faults shown in Fig. 3. The strike of these faults is estimated from reliable fault-plane solutions.

It is possible to estimate slip rates for these faults directly from the relative motions between GPS stations straddling them. Such information is available from McClusky *et al.* (2000), who interpreted GPS measurements of crustal motions for the period 1988–1997. These measurements were taken at 147 sites extending east–west from the Caucasus Mountains to the Adriatic Sea, and north–south from the southern edge of the Eurasian plate to the northern edge of the African plate. According to these authors, the southern Aegean as viewed from a Eurasia-fixed reference frame is characterized by coherent motion towards the southwest at $\sim$30 mm yr^{-1} relative to Eurasia. Internal deformation in the south Aegean plate is $<$2 mm yr^{-1}. The North Aegean Trough (NAT) region is the boundary between the Eurasian and south Aegean plates. Right-lateral strike-slip motion associated with the North Anatolian Fault (NAF) appears to become more distributed in the northern Aegean Sea, which is characterized by a combination of right-lateral shear and extension. Right-lateral deformation in the Aegean terminates at the Gulf of Corinth extensional system, which separates extension in the eastern gulf from the coherent translation of the southern Aegean. The earthquake focal mechanisms in the northern Aegean indicate that this relative motion is accommodated by NE-striking right-lateral strike-slip faults (i.e. deformation associated with the extension of the NAF into the northern Aegean). While

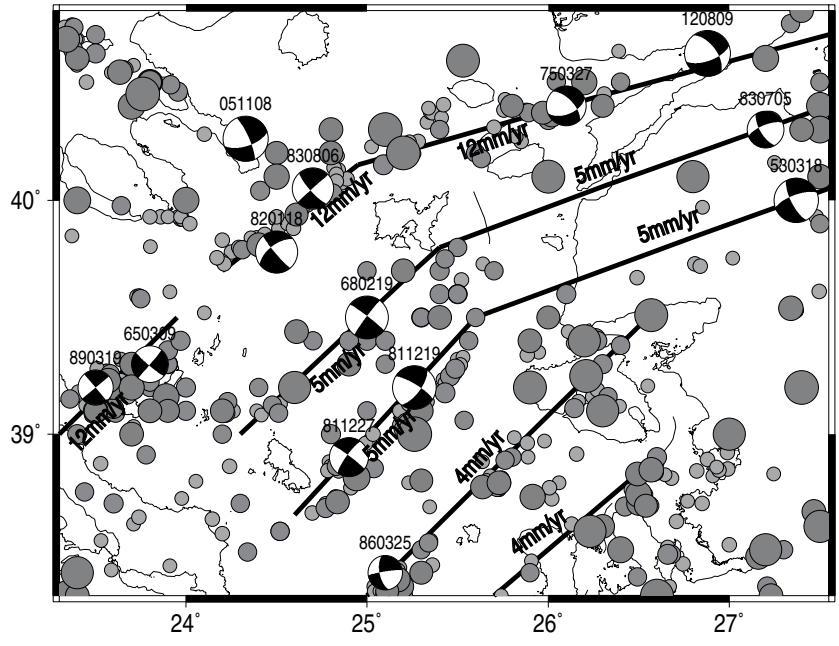

Figure 3. Major faults of the northern Aegean along with the recent seismicity (1981–1999) and representative focal mechanisms for the area. The occurrence date (year/month/date) of each event is given on top of the focal spheres.

the plate boundary region is characterized by large strike-slip motion, focal mechanisms indicate that some motion is accommodated by normal faults.

The GPS data indicate that motion between the southern Aegean and Eurasia plates is distributed across the northern Aegean, an interpretation that is supported by the distribution of earthquakes. Based on the motion of specific GPS stations, the long-term slip rates for each of these faults are defined approximately, so that their sum is in accordance with the generally accepted motion of the south Aegean microplate, up to 30 mm yr^{-1} to the southwest with respect to Eurasia. We assume then a total of 30 mm yr^{-1} of right-lateral slip, placing a large part of this motion (12 mm yr^{-1}) on the northern branch and distributing the rest along four other parallel faults, reducing the amount of slip from north to south. Information on the defined major faults and their inferred long-term slip rates are given in Fig. 3 and Table 1. In some places, it appears that the long-term slip rate is larger than the one derived by geodetic observations. Since we do not know the exact slip distribution, we tested the robustness of our results to variations in the distribution of slip rates. We put more slip on the northern fault (15 mm yr^{-1}) and reduced that on the other four parallel faults accordingly. We repeated the calculations in all stages of our evolutionary model and found that our results did not change appreciably. A probable reason for this is that the slip magnitudes (slip difference of the order of 0.28 m for 95 years) are considerably smaller than the modelled coseismic displacements in the larger events. Nevertheless, more accurate long-term rates for each fault that contribute to the total plate motion will undoubtedly promote better estimates of earthquake hazard.

4 FOCAL MECHANISMS OF LARGE EARTHQUAKES

Table 2 gives information on the fault-plane solutions of earthquakes with $M \geq 6.0$ that occurred in our study area during the 20th century. Reliable data on fault-plane solutions are available only for the strong earthquakes that occurred within the last four decades (Papazachos *et al.* 1998). Some large earthquakes, such as those of 1912 and 1953, produced primary surface rupture (Macovei 1912; Pinar 1953). Their mechanisms can be inferred from those observations along with additional information (spatial distribution of aftershock epicentres, macroseismic information).

Since a large uncertainty exists for even the epicentral locations of older earthquakes, their focal mechanism solutions are assigned using indirect information. Papazachos *et al.* (1999) used all the available information, such as fault-plane solutions, surface fault traces, spatial clustering of relatively small earthquakes and macroseismic observations, to define the fault parameters of 150 shallow strong ($M \geq 6.0$) earthquakes in the Aegean and surrounding areas. For those cases in which the rupture strike was determined from more than one technique, the modelled fault strike was selected on the basis of the quality of the original data. The dip and the rake reported are those determined for the fault-plane solution, if such information was available. When such a solution was not available, the dip and the rake of typical fault-plane solutions of smaller recent nearby earthquakes were adopted (Papazachos *et al.* 1998). The ambiguity of identifying the fault plane and auxiliary plane, when fault-plane solutions were available, was resolved using available additional seismological data (location of aftershocks, macroseismic effects, clustering, surface faulting) or other geological or topographic information. Thus, focal mechanism solutions for these older earthquakes were approximated using all available information.

Fault lengths and corresponding displacements from geological field observations are not available for the earthquakes studied. Rupture zones of several strong earthquakes in Greece have previously been defined using field observations of fault traces and precise locations of clusters of aftershocks or other relatively small earthquakes (location error less than 5 km). Such data have been used (Papazachos 1989) to derive the following relations between the fault length, L (in km), and mean displacement, u (in cm), as a function of the moment magnitude M:

$$\log L = 0.51M - 1.85\,, \tag{4}$$

$$\log u = 0.82M - 3.71\,. \tag{5}$$

We use these scaling laws to estimate the parameters L and u necessary for our model (Table 3).

The depths of the larger ($M \geq 6.0$) earthquakes that occurred in the broader Aegean region, for which reliable determination of the focal parameters exists based either on waveform inversion or on recordings of local seismic networks, range from 8 to 13 km (Papazachos *et al.* 1998). From studies of aftershock sequences for which reliable determinations of the aftershock focal parameters also exist, it is evident that the majority of their foci are located in a seismogenic layer extending from a

Table 1. Slip rates used for major fault segments in the northern Aegean Sea.

Segment number	Centre		Strike (°)	Dip (°)	Length (km)	Depth (km)	Fault type	Slip rate (mm yr^{-1})
	Lat (°N)	Long (°E)						
1	40.53	25.26	70	60	230	0–15	RL	12
2	39.92	24.58	50	80	80	0–15	RL	12
3	39.25	23.65	50	80	80	0–15	RL	12
4	39.40	24.85	40	87	130	0–15	RL	5
5	40.10	26.45	70	80	196	0–15	RL	5
6	39.08	25.10	40	87	128	0–15	RL	5
7	39.78	26.57	70	80	180	0–15	RL	5
8	38.95	25.83	75	40	188	0–15	RL	4
9	38.57	26.10	75	40	100	0–15	RL	4

Table 2. Source parameters of $M \geq 6.0$ earthquakes that occurred in the northern Aegean Sea during the 20th century and of some smaller ($5.5 \leq M \leq 6.0$) recent events.

Date	Time	Lat (°N)	Long (°E)	Depth (km)	M	Mechanism			Ref
						Strike	Dip	Rake	
1905, Nov 8	223030	40.26	24.33	0	7.1*	72	64	−167	1
1912, Aug 9	012900	40.62	26.88	0	7.6	70	64	−145	2
1912, Aug 10	092353	40.6	27.2	0	6.2	70	64	−145	2
1912, Sep 13	233124	40.1	26.8	0	6.7	256	64	−145	*
1923, Dec 5	205635	40.0	23.4	0	6.4	40	64	−167	3
1935, Jan 4	144130	40.4	27.5	0	6.4	256	64	−145	*
1935, Jan 4	162005	40.3	27.5	0	6.3	256	64	−145	*
1944, Oct 6	023441	39.51	26.57	0	6.9	257	46	−127	*
1947, Jun 4	002948	40.0	24.0	0	6.1	50	64	−167	*
1949, Jul 23	150330	38.58	26.23	0	6.7	250	46	−127	1
1953, Mar 18	190616	40.0	27.4	7	7.4	250	70	−160	4
1964, Apr 29	042105	39.2	23.7	20	6.0	45	89	179	*
1965, Mar 9	175754	39.3	23.8	14	6.1	40	89	−6	3
1967, Mar 4	175809	39.2	24.6	8	6.6	98	54	−107	3
1968, Feb 19	224542	39.5	25.0	9	7.5*	217	86	175	5
1975, Mar 27	051508	40.4	26.1	15	6.6	68	55	−145	6
1981, Dec 19	141051	39.2	25.26	8	7.2	37	67	−166	7
1981, Dec 27	173913	38.9	24.9	8	6.5	216	79	175	6
1982, Jan 18	192725	39.78	24.5	9	7.0	233	62	−173	6
1983, Jul 5	120127	40.3	27.2	10	6.1	248	70	−155	8
1983, Aug 6	154352	40.05	24.7	8	6.8	138	78	−1	9
1986, Mar 25	014135	38.4	25.1	3	5.7	261	84	−153	10
1989, Mar 19	053659	39.2	23.5	10	5.8	230	90	180	9
1992, Jul 23	201245	39.8	24.4	15	5.5	267	41	−160	9
1994, May 24	020534	38.8	26.5	21	5.6	258	54	−135	9

1: Papazachos 2: Ambraseys 3: Papazachos *et al.* (1998); ***:** Typical fault-plane solution for the area as determined by Papazachos *et al.* (1998); 4: Richter (1958); 5: Kiratzi *et al.* (1991); 6: Taymaz *et al.* (1991); 7: Papazachos *et al.* (1984); 8: Dziewonski *et al.* (1984); 9: Harvard solution; 10: NEIC determination.

depth of 3 to 15 km, some reaching a depth of 20 km. Although precise depth determination is not feasible for the smaller earthquakes in our study area, most of them are shallower than 15 km. Considering all of the above information, the depth of the seismogenic layer in our calculations is taken to be in the range of 3 to 15 km for all of the large ($M \geq 7.0$) events we modelled.

5 STRESS EVOLUTION AND TRIGGERING OF PAST AND FUTURE LARGE EVENTS

Stress changes, i.e. values of ΔCFF, are computed for typical faults in the northern Aegean, that is, vertical strike-slip faults orientated NE. Initial values of ΔCFF are assumed to be zero everywhere on each fault plane just before the 1905 earthquake. The poor quality of data prior to 1905 means we cannot extend calculations any farther back in time. In our model the cumulative stress change for every location is a result of the interaction between all of the faults described in Table 1 and the rupture models of the large ($M \geq 7.0$) earthquakes that occurred between 1905 and 1999 (Table 3). The shear modulus and Poisson's ratio are fixed as 33 GPa and 0.25, respectively. The apparent coefficient of friction, μ, is fixed as 0.6. Deng & Sykes (1997a,b) discussed this matter extensively and found similar results that were not very sensitive to changes in μ. Nalbant *et al.* (1998) selected a value for μ of 0.4, commenting that King *et al.* (1994) found that substantial variations from such a value do not greatly alter the distribution of Coulomb

Table 3. Rupture models for large earthquakes included in the evolutionary stress models.

Date	Time	Lat (°N)	Long (°E)	Depth (km)	L (km)	u (cm)	M	Mechanism		
								Strike	Dip	Rake
1905, Nov 8	223030	40.26	24.33	3–15	60	130	7.1*	72	64	−167
1912, Aug 9	012900	40.62	26.88	3–15	110	332	7.6	70	64	−145
1953, Mar 18	190616	40.0	27.4	3–15	84	228	7.4	250	70	−160
1968, Feb 19	224542	39.5	25.0	3–15	94	275	7.5*	217	86	+175
1981, Dec 19	141051	39.2	25.26	3–15	66	156	7.2	37	67	−166
1982, Jan 18	192725	39.78	24.5	3–15	52	107	7.0	233	62	−173

stresses around a fault. Stein *et al.* (1997) indicated that, in general, the changes in absolute values of μ are not great. Therefore, our value of 0.6 should be sufficient for our study.

In addition to the mainly strike-slip events that are listed in Table 3 and that are included in our evolutionary model, large normal faulting events have occurred in our study area during the 20th century. We computed the ΔCFF both with and without the coseismic displacement of the largest one, the 1919 November 18, Soma–West Turkey event of $M=7.0$. Its strike of 98°, dip of 45° and rake of −97° are taken from Papazachos & Papazachou (1997). The maximum difference between the two ΔCFF calculations was less than 0.01 bar. Because a value of 0.01 bar does not appreciably modify our results, large normal faulting events are not included in our calculations. Moreover, the two larger normal faulting events of the 20th century, the 1919 shock and that of 1944 of $M=6.8$ are located in western Turkey, near the edge of our study area and we therefore expect their contribution to ΔCFF to be less than 0.01 bar.

Figs 4(a) to (l) are snapshots of ΔCFF at a depth of 8.0 km. This depth, the choice of which is not very critical since the faults are almost vertical, was chosen to be several kilometres above the locking depth in the evolutionary model. In these figures, dark regions denote negative changes in CFF and inferred decreased likelihood of fault rupture. These regions are called stress shadows (Harris & Simpson 1993, 1996). Light regions represent positive ΔCFF and increased likelihood of fault rupture. The positive ΔCFF regions are called stress bright zones. It should be noted that stress is a tensorial, not a scalar, quantity, and thus shadow zones and bright zones must be viewed in the context of a specific style of fault slip, i.e. strike, dip and rake. A particular location could be situated in a shadow zone for NE-trending strike-slip faults, while it could be located in a bright zone for other styles of faulting. We will show that, in the stress evolutionary calculations, most of the larger earthquakes therefore occurred in bright zones, not in shadow zones. Moreover, moderate-sized shocks of strike-slip faulting for which the stress calculations were performed were also located in stress-enhanced zones.

The coseismic displacements for the six largest earthquakes in the northern Aegean Sea since the beginning of the 20th century, namely those with $M\geq7.0$ (Table 3), are included in the evolutionary stress model. The faults are simplified and approximated by rectangular shapes. All of these events involve mainly strike-slip faulting with fault planes orientated in a NE–SW direction. At each stage, ΔCFF is calculated for a preferred fault-plane solution, that of the next inspected event. The changes in stress are presented for the whole area of the northern Aegean Sea. Events involving normal faulting are omitted for the reasons outlined above.

5.1 Earthquake of 1905

Fig. 4(a) shows the coseismic stress changes associated with the large earthquake of 1905 ($M=7.1$). A displacement of 1.3 m and a fault length of 60 km are used. Rupture is taken to extend throughout the seismogenic zone, namely from 3 to 15 km. This earthquake created a shadow zone in the western part of our study area and a bright zone in the central part. We expect these stress changes to affect the occurrence of future events.

5.2 Earthquake of 1912

A great earthquake of magnitude 7.6 occurred in 1912 along the western part of one of the main branches of the North Anatolian fault. Figs 4(b) and (c) show the state of stress before and after this earthquake with respect to the 1905 baseline. The shadow zone created by the 1905 event is eliminated over time as stress accumulates from 1905 to 1912. Just prior to the 1912 event, a broad zone of positive ΔCFF was created (Fig. 4b) that covered the central and most eastern parts of our study area. The rupture zone of the main 1912 event along with those of the two strong ($M\geq6.5$) earthquakes that occurred in the next few days were located in the large region of positive ΔCFF.

In Fig. 4(b) the epicentres of all the known $M\geq6.5$ earthquakes that occurred in the northern Aegean Sea during the time interval 1845–1893 are plotted as stars. It is worth noting that the epicentres of most of these events, even considering errors in location (±20 km) (Papazachos & Papazachou 1997), are situated in the central and eastern parts of this bright zone. One could ask why the central and southern parts of this bright zone did not experience a large event, since the calculated state of Coulomb stress is about the same level as that for when the 1912 seismic sequence took place. A possible explanation is that part of this bright zone should be considered to be in the stress shadow resulting from the large events that occurred in the second half of the 19th century. In addition, some of these epicentres may be located towards the island of Lesvos, since their location is based on macroseismic information concerning damage in urban areas on the island. The next large earthquakes (in 1912) occurred in the northeastern part of the area, which had an absence of known large earthquakes in the 19th century.

Modelled stress evolution after 1905 includes the coseismic stress changes associated with the 1912, $M=7.6$ event (Fig. 4c). A large shadow zone covering the eastern part of our study area was created during this time, while the central part of the area remained a bright zone.

5.3 Earthquake of 1953

Fig. 4(d) shows the accumulated Coulomb stress changes just before the 1953 earthquake calculated according to its fault-plane solution. By 1953 a large bright zone had been created running along the central part of the study area, a branch of which includes the rupture zone of the 1953 event. Focal mechanism solutions for all the earthquakes with $M\geq6.0$ that occurred after the 1912 and before the 1953 earthquakes are also plotted in this figure. Note that the 1923 and 1935 events, which are mainly strike-slip, are also located in bright zones. The strike-slip event of 1947 is located at the border between bright and shadow zones, making triggering by ΔCFF doubtful. We did not, however, take into account uncertainties in epicentral location. After the 1953 event, a large shadow zone occupied the eastern part of the study area, while the bright zone that covered the central and western parts remained largely unaffected (Fig. 4e).

5.4 Earthquake of 1968

In Fig. 4(f) the accumulated Coulomb stress changes just before the 1968 event are shown for faulting in agreement with its focal mechanism solution. The fault-plane solutions of all events with

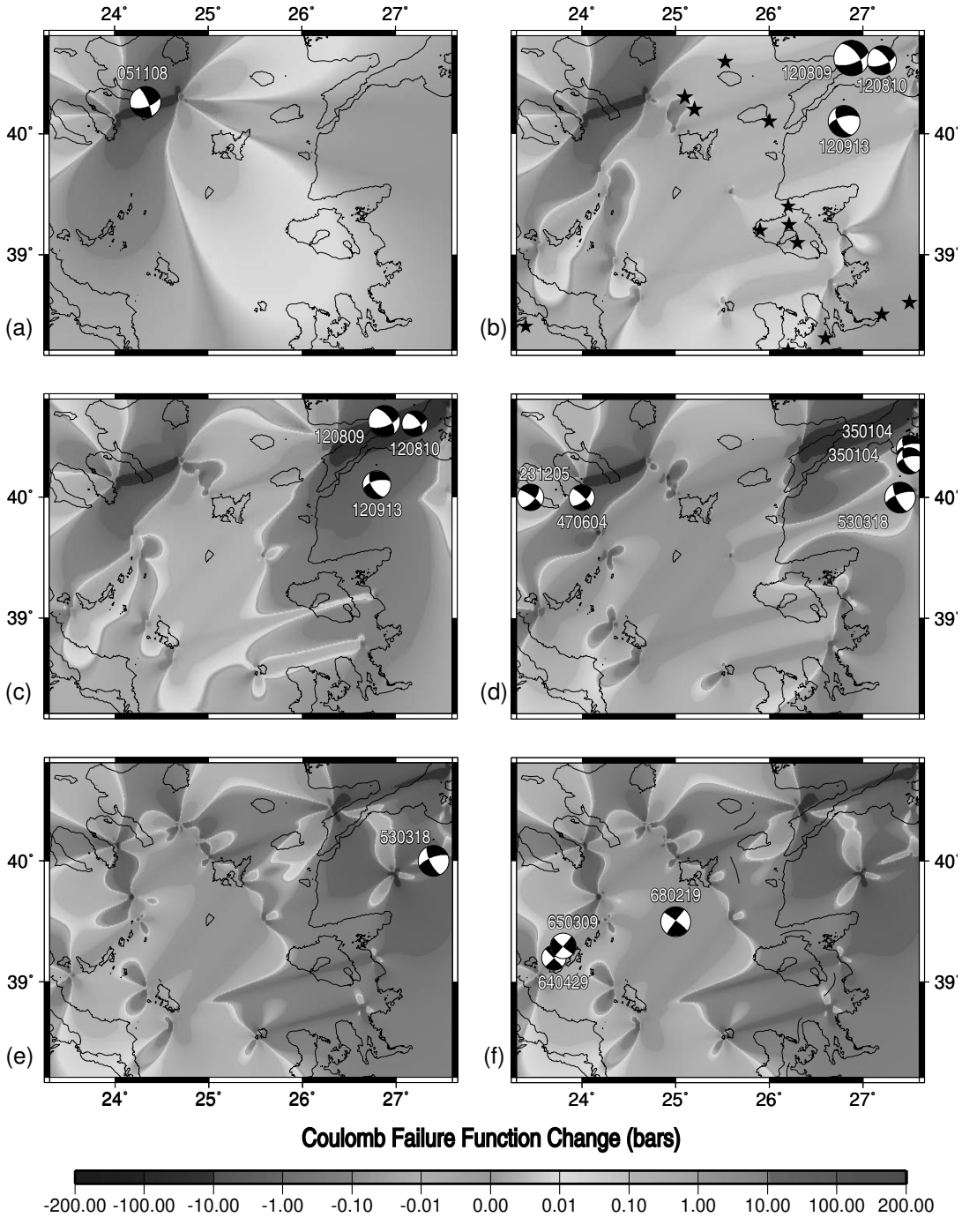

Figure 4. Stress evolution in the northern Aegean area since 1905. Coulomb stress is calculated for strike-slip faults at a depth of 8.0 km. The stress pattern is calculated for the faulting type of the next large event in the sample. Changes are denoted by the greyscale at the bottom (in bars). The Coulomb failure function (ΔCFF) is taken to be zero everywhere before the earthquake of 1905. Fault-plane solutions are plotted as lower-hemisphere equal-area projections. Annotation of the occurrence date as in Fig. 3. (a) Coseismic Coulomb stress changes associated with the 1905 event. (b) Stress evolution until just before the 1912 events. Stars denote epicentres of known events with $M > 6.5$ that occurred from 1845 to 1893. (c) ΔCFF just after the 1912 main event. Coseismic stress changes associated with that earthquake as well as additional tectonic stress changes included since 1905 are included. Focal mechanisms of earthquakes that constitute the 1912 seismic sequence are also shown. (d) Stress evolution until just before the occurrence of the 1953 event and focal mechanisms of earthquakes from 1913 to 1953. (e) State of stress just after the 1953 event. (f) Stress evolution just before the occurrence of the 1968 event, and focal mechanisms of the events that occurred between 1953 and 1968. (g) ΔCFF just after the 1968 event. (h) State of stress just before the occurrence of the 1981 events. (i) Stress evolution after the 1981 events, and the fault-plane solution of the 1982 event. (j) ΔCFF right after the 1982 event. (k) Stress evolution as of 1999, and reliable fault-plane solutions for events that occurred between 1982 and 1999. Note that the events with optimally orientated faults occur in bright zones ($\Delta CFF > 0$) or near the borders between bright and shadow zones ($\Delta CFF \approx 0$). (l) Evolution of stress in 2020 assuming that no large earthquakes occur between 1999 and 2020. Mechanisms and large bright zones indicate possible sites of future large earthquakes. The mechanisms shown are those of the typical strike-slip fault-plane solutions for the area of the northern Aegean. The stress field was calculated for this fault-plane solution. Fig. 4 may be viewed in colour in the online version of the journal (http://www.blackwell-synergy.com).

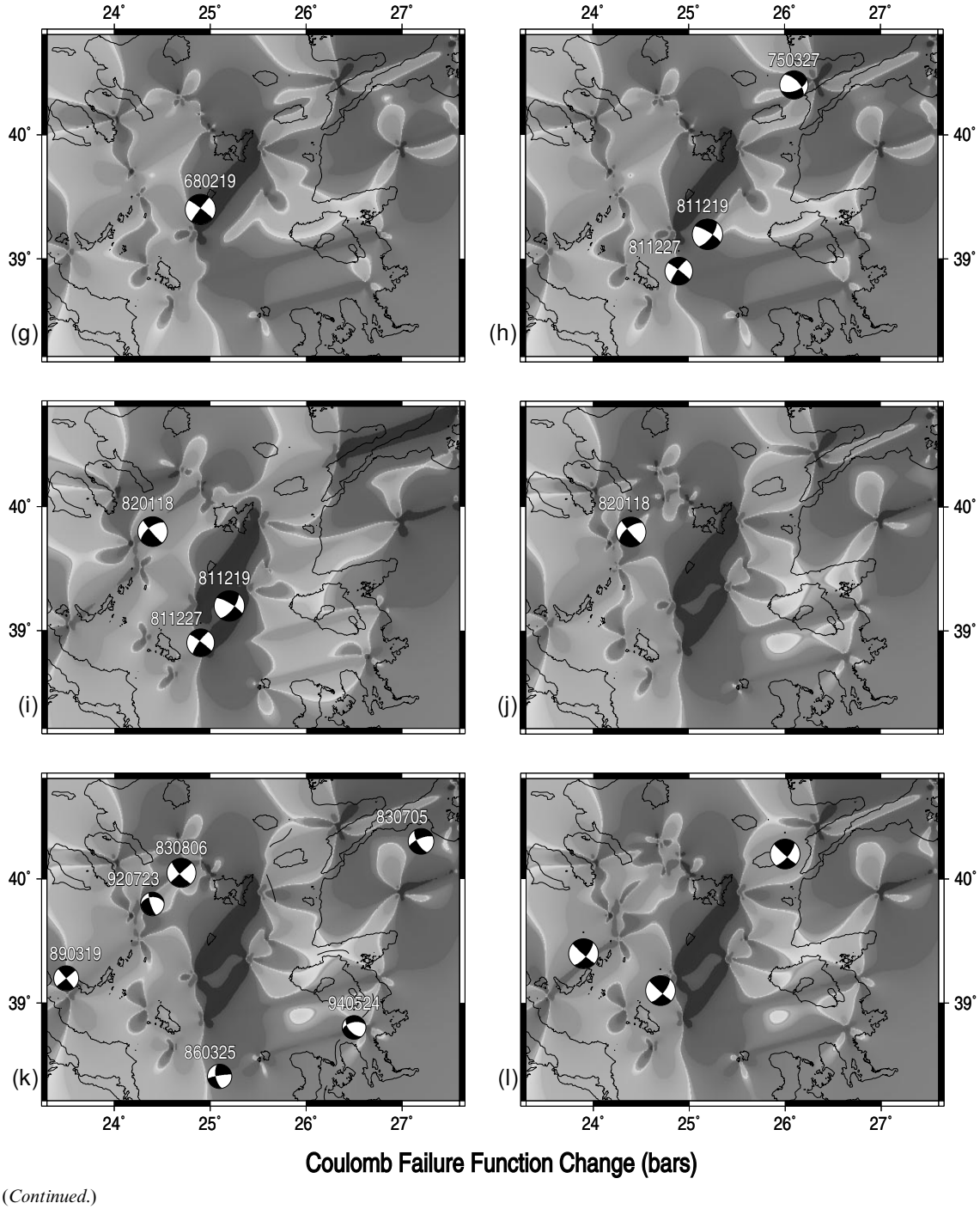

Figure 4. (*Continued.*)

$M \geq 6.0$ that occurred from 1953 to 1968 are also shown. All are located in bright zones. The large ($M = 7.2$) event of 1968 occurred in the middle of the largest bright zone in the region, where ΔCFF is most positive.

The state of ΔCFF just after the 1968 earthquake is shown in Fig. 4(g). Shadow zones, regions not expected to have future large events, now occupy a large part of the study area.

5.5 Earthquakes of 1981, 1982

Fig. 4(h) shows the accumulated Coulomb stress changes just before the 1981 earthquakes. The main shock of this seismic sequence of $M = 7.2$ occurred on 1981 December 19, and its largest aftershock of $M = 6.5$ just a week later (1981 December 27). The epicentres of both events are located along the borders of the shadow zone created by the large event of 1968. This is an indication that perhaps the occurrence of the 1968 shock may have postponed the occurrence of the 1981 sequence. The same figure shows the fault-plane solution, a combination of strike-slip and normal faulting, of the 1975 event of $M = 6.5$. Its rupture zone is located in a patch of the bright zone that remained largely unaffected by the occurrence of the 1968 event.

The stress pattern after the 1981 earthquake is calculated for the fault-plane solution of the 1982 event (Fig. 4i). The stress

shadow is now limited to a narrow zone in the central part of our study area. The bright zones caused by the 1981 event moved parts of the study area closer to failure or contributed to the enlargement of existing bright zones. In Fig 4(i), the fault-plane solution of the $M=7.0$ event of 1982 is plotted. It occurred on 1982 January 18, just one month after the two events of 1981. The 1982 earthquake is another example of an earthquake whose epicentre occurred in a bright zone.

The addition of coseismic stress changes associated with the occurrence of the 1982 event are shown in Fig. 4(j). The central part of our study area, where the events of 1981 and 1982 occurred, is now covered by a stress shadow.

5.6 State of stress in 1999

After 1982 no large event ($M>7.0$) occurred in our study area until 1999. The snapshot of Fig. 4(k) indicates the evolved state of stress as of 1999, which differs from that of Fig. 4(j) in that it includes the stress accumulation caused by 17 additional years of tectonic loading. Hence, stresses are derived for a typical strike-slip fault plane for the area (strike 40°, dip 70° and rake 180°). The focal mechanisms of strike-slip events occurring between 1982 and 1999 of $M\geq6.0$ are also shown. The event of 1983 August 6 ($M=6.8$) is located in a well-defined bright zone enhanced by the occurrence of the 1982 event. As for the shock of 1983 July 5 ($M=6.1$), it is well located in a shadow zone. However, we have to consider that, since that event was located near the border of our study area, the pattern in Fig. 4(j) does not include the effect of nearby events that occurred outside our study area. For example, we do not include the recent large Izmit earthquake in the Marmara Sea (1999 August 17, $M=7.4$), which may move the northeastern part of our study area slightly (less than 0.1 bar) closer to failure.

5.7 Calculations for 2020

The Coulomb stress evolutionary calculations have been continued until 2020 assuming no large earthquakes occur until then (Fig. 4l). Displacement is assumed to be the slip accumulated since the occurrence of the last large earthquake on each fault segment. Candidate future earthquakes of $M\geq6.5$ are shown as focal mechanisms in Fig. 4(l). The bright zones represent possible sites of future large strike-slip events in the western and northeastern parts of the area under examination. A large strike-slip earthquake east of the 1912 and west of the 1999 Izmit rupture zones could move strike-slip faults in our study area closer to failure.

6 DISCUSSION AND CONCLUSIONS

Many models of static or dynamic stress changes influencing subsequent earthquake occurrence are for a particular tectonic setting and for one earthquake cycle or less (Das & Scholz 1981; Stein & Lisowski 1983; Harris & Simpson 1992; Reasenberg & Simpson 1992; Toda *et al.* 1998; Belardinelli *et al.* 1999; Astiz *et al.* 2000; Cocco *et al.* 2000; Kilb *et al.* 2000). Some research has been conducted to evaluate longer-term effects, including multiple earthquake cycles (Goes 1996; Yamashita 1995; Ward 1992; Ward & Goes 1993; Robinson & Benites 1996) by examining the recurrence of large ($M\geq7$) earthquakes, using synthetic seismicity models or simulating earthquake statistics. All of these studies found that fault (earthquake) interactions significantly changed the timing (and locations) of the simulated events.

The area of our study is one of the most active areas in the broader Aegean region. Strong ($M\geq6.5$) events occur here frequently and tend to be clustered in time and in space. An example of a recent cluster is the sequence of four events with $M\geq6.5$ that took place within less than two years (1981–1983). Since models assuming tectonic loading alone cannot explain their sequential occurrence, fault interaction leading to the triggering of one event by a previous one or ones could be a probable mechanism for their occurrence.

To model the evolution of the stress field, we had to make several assumptions about the nature of strain accumulation and release in our study area and to ignore some potentially important features. Chief among these assumptions are: (1) that the time-predictable model describes the cycle of stress accumulation and release in the vicinity of very active faults; (2) that strain accumulation is linear with time; (3) that earthquakes of $M<7.0$ do not appreciably modify the stress field; (4) that the five fault segments we modelled account for most of the changes in the stress field in the study area; (5) that a zero base line of ΔCFF can be assumed for 1905, the start date of our study; and (6) that aseismic deformation and changes in stress resulting from rate-state behaviour can be neglected. We know that differences in crustal structure, non-elastic changes, and rate-state friction should be incorporated in future models. Incorporating them will require years of work, since programs to include them are still in their infancy, as is our knowledge of non-elastic and rate-state parameters. The problem of stress diffusion needs to be addressed, and so do temporal changes related to rate and state frictional parameters.

The evolution of stress in our study area was modelled for the time interval 1905–1999 using a series of dislocations in an elastic half-space to represent tectonic stress build-up along major faults as well as coseismic stress changes from large ($M\geq7.0$) earthquakes. Tectonic loading on the major faults is assumed to occur continuously at their long-term slip rates as derived from geodetic (GPS) measurements. Interseismic tectonic strain accumulation acts to eliminate the stress shadow of a large or great earthquake with time, thus bringing regional faults back to or close to their stress levels just prior to those large earthquakes.

The coseismic stress change induced by a large earthquake is modelled by imposing slip of the correct sense and magnitude on the fault segment(s) involved such as to fit the observed mechanism and seismic moment. The Coulomb failure function, ΔCFF, was calculated for strike-slip faults, which is the dominant faulting type of the area, and is calculated just before and just after the occurrence of each large event. We found that the stress on strike-slip faults is not appreciably modified by the coseismic displacement of the large dip-slip events that occurred in the study area during the investigated period. At each stage, the stress pattern was calculated for the strike, dip, and rake of faulting in the next large event. While stress often decreased in the vicinity of these large events, localized areas existed where ΔCFF was enhanced, i.e. faults were moved closer to failure. In those areas of enhanced stress, areas of positive ΔCFF, the next large event typically occurred. Although we did not include the coseismic stress changes of earthquakes with $M\leq7.0$ in our

stress model, we find that large earthquakes produce changes in the state of stress of sufficient magnitude (more than 0.1 MPa) to modify seismicity in the region.

One of our assumptions is the linear dependence of strain accumulation on time. Geodetic measurements of deformation in the San Francisco Bay region show, however, that the regional strain rate apparently was elevated in the 20–40 years following the 1906 earthquake (Thatcher 1983; Gilbert *et al*. 1993). Two mechanisms have been proposed to account for this behaviour: (1) the relaxation of a viscous layer beneath the seismogenic portion of the crust (Savage & Prescott 1978); and (2) transient post-seismic slip on the fault below the earthquake rupture (Thatcher 1983). Both models can account for the observed changes in shear strain rates following the 1906 earthquake (Thatcher 1983). Stein *et al*. (1992) found that stress changes on the southern San Andreas fault system caused by the Landers earthquake, as well as the relaxation of a viscous layer beneath the brittle crust, lead to an increase in the stress change on nearby faults. Jaumé (1994) modelled the effect of deep post-seismic slip on the evolution of the stress field and found that it also reinforces the stress change imposed by the causative earthquake. Thus, it appears that both of these post-seismic deformation processes act to reinforce the stress changes caused by coseismic slip. The post-seismic transient slip below the seismogenic layer after a large earthquake, which is a time-dependent process, may also act to reinforce the regional stress changes. These time-dependent processes are likely to be most important in the few years (decades) following a great earthquake (Freed & Lin 1998). Although these processes account for the evolution of the stress field, along with differences in crustal structure, non-elastic changes, and rate-state friction, they are not incorporated in our model. The problem of stress diffusion as well as temporal changes related to rate and state frictional parameters need to be addressed in future work. We used instead a purely elastic model, which, despite its simplicity, proved to be very effective in predicting the locations of future earthquakes. Similar calculations for southern California by Deng & Sykes (1997a,b) show a very good correlation between positive values of ΔCFF and the distribution of large shocks of the past 185 years, moderate-sized shocks of the past few decades, and small and microearthquakes for a more recent time period for which data are available. In this paper, we are also effective in predicting the sites of 20th century large earthquakes in our study area.

By extrapolating our calculations to the next 20 years, we suggest three sites in our study area where large events are more likely to occur. Two of these sites are located in the western part of the area, while the third one is located in the Gulf of Saros, namely the area near the 1912 and 1975 earthquakes. A previous study concerning fault interaction was made for this region by Nalbant *et al*. (1998). Their model differs from ours in that it does not include tectonic loading and makes assumptions about the directions and magnitudes of regional stresses. Tectonic loading contributes 3 m per century of potential slip across the study area. In addition, they consider strike-slip faults and dip-slip ones to contribute to stress changes. One of the probable sites found in our study, namely the Gulf of Saros, was also identified by them as a candidate location for the occurrence of a future large ($M \geq 6.5$) event.

Maps of the current stress field can provide additional information for long-term earthquake prediction. During the next few decades, we expect that earthquakes may well occur in one or more of the areas of positive ΔCFF. This is an illustration of earthquake triggering. Triggering does not mean that the coseismic stress change associated with one earthquake is enough to generate another earthquake at an originally stress-free location; it means that stresses at the location of the second earthquake are already close enough to failure that the first earthquake can 'trigger' the second one by introducing a positive increase in ΔCFF such as to move it into the failure regime.

ACKNOWLEDGMENTS

The stress tensors were calculated using a program written by J. Deng (Deng & Sykes 1997a) using the DIS3D code of S. Dunbar and Erikson (1986) and the expressions of G. Converse. W. X. Du of Lamont helped us to use Deng's program. The GMT system (Wessel & Smith 1991) was used to plot the figures. The manuscript benefited from the review of Debi Kilb and an anonymous reviewer. This work was started and part of it was implemented when the first author was a visitor at Lamont-Doherty Earth Observatory. She would like to express her sincere gratitude for the fruitful discussions she had with colleagues from the Seismology Section and the warm environment she found from all the staff. This is Department of Geophysics contribution 560 and Lamont-Doherty Earth Observatory contribution 6223.

REFERENCES

Aki, K. & Richards, P., 1980. *Quantitative Seismology: Theory and Methods,* W. H. Freeman, San Francisco.

Ambraseys, N.N. & Finkel, C.F., 1987. Seismicity of Turkey and neighboring regions, 1899–1915, *Ann. Geophys.,* **5,** 701–726.

Astiz, L., Shearer, P.M. & Agnew, D.C., 2000. Precise relocations and stress change calculations for the Upland earthquake sequence in southern California, *J. geophys. Res.,* **105,** 2937–2953.

Belardinelli, M.E., Cocco, M., Coutant, O. & Cotton, F., 1999. Redistribution of dynamic stress during coseismic ruptures: Evidence for fault interaction and earthquake triggering, *J. geophys. Res.,* **104,** 14 925–14 945.

Beroza, G.C., 1991. Near-source modeling of the Loma-Prieta earthquake; evidence for heterogeneous slip and implications for earthquake hazard, *Bull. seism. Soc. Am.,* **81,** 1603–1621.

Cocco, M., Nostro, C. & Ekström, G., 2000. Static stress changes and fault interaction during the 1997 Umbria-Marche earthquake sequence, *J. Seismol.,* **4,** 501–516.

Das, S. & Scholz, C., 1981. Theory of time-dependent rupture in the earth, *J. geophys. Res.,* **86,** 6039–6051.

Deng, J. & Sykes, L.R., 1997a. Evolution of the stress field in southern California and triggering of moderate-size earthquakes: a 200-year perspective, *J. geophys. Res.,* **102,** 9859–9886.

Deng, J. & Sykes, L.R., 1997b. Stress evolution in southern California and triggering of moderate-, small-, and micro-size earthquakes, *J. geophys. Res.,* **102,** 24 411–24 435.

Dziewonski, A., Franzen, J. & Woodhouse, J., 1984. Centroid–moment tensor solutions for July–September, 1983, *Phys. Earth planet. Inter.,* **34,** 1–8.

Erikson, L., 1986. User's manual for DIS3D: A three-dimensional dislocation program with applications to faulting in the Earth, *MSc thesis,* Stanford University, Stanford, CA.

Freed, A.M. & Lin, J., 1998. Time-dependent changes in failure stress following thrust earthquakes, *J. geophys. Res.,* **103,** 24 393–24409.

Gilbert, L.E., Beavan, J. & Scholz, C.H., 1993. Analysis of a 100 year geodetic record from northern California, in *Contributions of Space Geodesy to Geodynamics: Crustal Deformation, Geodyn. Ser. 23,* pp. 215–232, eds Smith, D.E. & Turcotte, D.L., Am. geophys. Un., Washington, DC.

Goes, S.D.B., 1996. Irregular recurrence of large earthquakes: An analysis of historic and paleoseismic catalogs, *J. geophys. Res.,* **101,** 5739–5749.

Harris, R.A., 1998. Introduction to special section: Stress triggers, stress shadows, and implications for seismic hazard, *J. geophys. Res.,* **103,** 24 347–24 358.

Harris, R.A. & Simpson, R.W., 1992. Changes in static stress on southern California faults after the 1992 Landers earthquake, *Nature,* **360,** 251–254.

Harris, R.A. & Simpson, R.W., 1993. In the shadow of 1857: An evaluation of the static stress changes generated by the M8 Ft. Tejon, California, earthquake, *EOS, Trans. Am. geophys. Un.,* **74** (43), 427.

Harris, R.A. & Simpson, R.W., 1996. In the shadow of 1857: The effect of the great Ft. Tejon earthquake on subsequent earthquakes in southern California, *Geophys. Res. Lett.,* **23,** 229–232.

Harris, R.A. & Simpson, R.W., 1998. Suppression of large earthquakes by stress shadows: a comparison of Coulomb and rate-and-state failure, *J. geophys. Res.,* **103,** 24 439–24 452.

Jackson, J., 1994. Active tectonics of the Aegean region, *Ann. Rev. Earth planet. Sci.,* **22,** 239–271.

Jaumé, S.C., 1994. Earthquakes in an evolving stress/strain field, *PhD thesis,* Columbia University, New York.

Jaumé, S.C. & Sykes, L.R., 1996. Evolution of moderate seismicity in the San Francisco Bay region, 1850–1993: Seismicity changes related to the occurrence of large and great earthquakes, *J. geophys. Res.,* **101,** 765–789.

Kilb, D., Gomberg, J. & Bodin, P., 2000. Triggering of earthquake aftershocks by dynamic stresses, *Nature,* **408,** 570–574.

King, G.C.P., Stein, R.S. & Lin, J., 1994. Static stress changes and the triggering of earthquakes, *Bull. seism. Soc. Am.,* **84,** 935–953.

Kiratzi, A.A., Wagner, G. & Langston, C.A., 1991. Source parameters of some large earthquakes in Northern Aegean determined by body waveform inversion, *Pure appl. Geophys.,* **135,** 515–527.

LePichon, X., Chamot-Rooke, N., Lallemant, S., Noomen, R. & Veis, G., 1995. Geodetic determination of the kinematics of central Greece with respect to Europe: Implications for eastern Mediterranean tectonics, *J. geophys. Res.,* **100,** 12 675–12 690.

Lienkaemper, J.J., Galehouse, J.S. & Simpson, R.W., 1997. Creep response of the Hayward fault to stress changes caused by the Loma Prieta earthquake, *Science,* **276,** 2014–2016.

McClusky, S. *et al.*, 2000. GPS constraints on crustal movements and deformations in the Eastern Mediterranean (1988–97): Implications for plate dynamics, *J. geophys. Res.,* **105,** 5695–5719.

McKenzie, D.P., 1970. The plate tectonics of the Mediterranean region, *Nature,* **226,** 239–243.

McKenzie, D.P., 1972. Active tectonics of the Mediterranean region, *Geophys. J. R. astr. Soc.,* **30,** 109–185.

McKenzie, D.P., 1978. Active tectonics of the Alpine-Himalayan belt: the Aegean Sea and surrounding regions, *Geophys. J. R. astr. Soc.,* **55,** 217–254.

Macovei, G., 1912. About the Sea of Marmara earthquake of the 9 August, 1912, *Bull. Sect. Sci. Acad. Roumanie, Bucarest,* **1,** 1–10 (in French).

Nalbant, S.S., Hubert, A. & King, G.C.P., 1998. Stress coupling between earthquakes in northwestern Turkey and the north Aegean sea, *J. geophys. Res.,* **103,** 24 469–24 486.

Okada, Y., 1992. Internal deformation due to shear and tensile faults in a half-space, *Bull. seism. Soc. Am.,* **82,** 1018–1040.

Oral, M.B., Reilinger, R.E., Toksoz, M.N., King, R.W., Barka, A.A. & Kinik, I., 1995. Coherent plate motions in the eastern Mediterranean continental collision zone, *EOS, Trans. Am. geophys. Un.,* **76,** 9–11.

Papazachos, B.C., 1989. Measures of earthquake size in Greece and surrounding areas, *Proc. 1st Sci. Cong., Geophys. Soc. Greece,* pp. 438–447.

Papazachos, C.B., 1999. Seismological and GPS evidence for the Aegean–Anatolia interaction, *Geophys. Res. Lett.,* **26,** 2653–2656.

Papazachos, B.C. & Comninakis, P.E., 1970. Geophysical features of the Greek island arc and eastern Mediterranean ridge, *Com. Ren. Des Sceances la Conf. Reunie a Madrid,* 16, pp. 74–75.

Papazachos, B.C. & Comninakis, P.E., 1971. Geophysical and tectonic features of the Aegean arc, *J. geophys. Res.,* **76,** 8517–8533.

Papazachos, C.B. & Kiratzi, A.A., 1996. A detailed study of the active crustal deformation in the Aegean and surrounding area, *Tectonophysics,* **253,** 129–153.

Papazachos, B.C. & Papazachou, C.B., 1997. *The Earthquakes of Greece,* Ziti Publishers, Thessaloniki.

Papazachos, B.C., Kiratzi, A.A., Voidomatis, Ph.S. & Papaioannou, ChA., 1984. A study of the December, 1981–January, 1982 seismic activity in northern Aegean Sea, *Boll. Geof. teor. appl.,* **26,** 101–113.

Papazachos, B.C., Papadimitriou, E.E., Kiratzi, A.A., Papazachos, C.B. & Louvari, E.K., 1998. Fault plane solutions in the Aegean Sea and the surrounding area and their tectonic implications, *Boll. Geof. teor. appl.,* **39,** 199–218.

Papazachos, B.C., Papaioannou, Ch.A., Papazachos, C.B. & Savvaidis, A.S., 1999. Rupture zones in the Aegean region, *Tectonophysics,* **308,** 205–221.

Papazachos, B.C., Comninakis, P.E., Karakaisis, G.F., Karakostas, B.G., Papaioannou, Ch. A., Papazachos, C.B. & Scordilis, E.M., 2000. A catalogue of earthquakes in Greece and surrounding area for the period 550 BC–1999, *Publ. Geophys. Lab., University Thessaloniki,* **1**.

Pavlides, S.B. & Tranos, M.D., 1991. Structural characteristics of two strong earthquakes in the North Aegean: Ierissos (1932) and Agios Efstratios (1968), *J. struct. Geol,* **13,** 205–214.

Pinar, N., 1953. The Yenice earthquake of 18 March, 1953 and the fracture line of Yenice-Gönen, *Rev. Fac. Sci. Univ. Istanbul, Ser. A,* **18,** 131–141.

Reasenberg, P.A. & Simpson, R.W., 1992. Response of regional seismicity to the static stress change produced by the Loma Prieta earthquake, *Science,* **255,** 1687–1690.

Reilinger, R.E., McClusky, S.C., Oral, M.B., King, R.W., Toksoz, M.N., Barka, A.A., Kinik, I., Lenk, O. & Sanli, I., 1997. Global Positioning System measurements of present-day crustal movements in the Arabia-Africa-Eurasia plate collision zone, *J. geophys. Res.,* **102,** 9983–9999.

Richter, C.F., 1958. *Elementary Seismology,* Freeman, San Fransisco.

Robinson, R. & Benites, R., 1996. Synthetic seismicity models for the Wellington region, New Zealand: Implications for the temporal distribution of large events, *J. geophys. Res.,* **101,** 27 833–27 844.

Savage, J.C. & Prescott, W.H., 1978. Asthenosphere readjustment and the earthquake cycle, *J. geophys. Res.,* **83,** 3369–3376.

Scholz, C., 1990. *The Mechanics of Earthquakes and Faulting,* Cambridge University Press, Cambridge.

Shimazaki, K. & Nakata, T., 1980. Time-predictable recurrence model for large earthquakes, *Geophys. Res. Lett.,* **7,** 279–282.

Simpson, R.W. & Reasenberg, P.A., 1994. Earthquake-induced static stress changes on central California faults, in *The Loma Prieta, California Earthquake of October 17, 1989—Tectonic Processes and Models,* ed. Simpson, R.W., *U.S. Geol. Surv. Prof. Pap.* 1550-F, F55–F89.

Simpson, R.W., Schulz, S.S., Dietz, L.D. & Burford, R.O., 1988. The response of creeping parts of the San Andreas fault to earthquakes on nearby faults: Two examples, *Pure appl. Geophys.,* **126,** 665–685.

Stein, R.S. & Lisowski, M., 1983. The 1979 Homestead Valley earthquakes sequence, California: Control of aftershocks and post-seismic deformation, *J. geophys. Res.,* **88,** 6477–6490.

Stein, R.S., King, G.L.P. & Lin, J., 1992. Change in failure stress on the southern San Andreas fault system caused by the 1992 magnitude = 7.4 Landers earthquake, *Science,* **258,** 1328–1332.

Stein, R., Barka, A. & Dieterich, J., 1997. Progressive failure on the North Anatolian fault since 1939 by earthquake stress triggering, *Geophys. J. Int.,* **128,** 593–604.

Steketee, J.A., 1958. On Voltera's dislocations in a semi-infinite elastic medium, *Can. J. Phys.,* **36,** 192–205.

Taymaz, T., Jackson, J. & McKenzie, D., 1991. Active tectonics of the north and central Aegean Sea, *Geophys. J. Int.,* **106,** 433–490.

Thatcher, W., 1983. Nonlinear strain buildup and the earthquake cycle on the San Andreas fault, *J. geophys. Res.,* **88,** 5893–5902.

Toda, S., Stein, R.S., Reasenberg, P.A., Dieterich, J.H. & Yoshida, A., 1998. Stress transferred by the 1995 $M_w = 6.9$ Kobe, Japan, shock: Effect on aftershocks and future earthquake probabilities, *J. geophys. Res.,* **103,** 24 543–24 565.

Ward, S.N., 1992. An application of synthetic seismicity calculations in earthquake statistics: the Middle America trench, *J. geophys. Res.,* **97,** 6675–6682.

Ward, S.N. & Goes, S.D.B., 1993. How regularly do earthquakes recur? A synthetic seismicity model for the San Andreas fault, *Geophys. Res. Lett.,* **20,** 2131–2134.

Wessel, P. & Smith, W.H.F., 1991. New version of the Generic Mapping Tools released, *EOS, Trans. Am. geophys. Un.,* **76,** 329.

Yamashita, T., 1995. Simulation of seismicity due to ruptures on noncoplanar interactive faults, *J. geophys. Res.,* **100,** 8339–8350.